# An Adaptive Approach to Mammographic Image Denoising and Enhancement

Jacob Scharcanski
UFRGS - Universidade Federal do Rio Grande do Sul
Caixa Postal 15064, 91501-970, Porto Alegre, RS, Brasil
jacobs@inf.ufrgs.br

Cláudio Rosito Jung
UNISINOS - Universidade do Vale do Rio dos Sinos
Ciências Exatas e Tecnológicas
Av. UNISINOS, 950. São Leopoldo, RS, Brasil, 93022-000
crjung@exatas.unisinos.br

## Abstract

*This paper describes a new method for mammographic image noise suppression and enhancement based on the wavelet transform. At each resolution, coefficients associated with noise are modelled by Gaussian random variables; coefficients associated with edges are modelled by Generalized Gaussian random variables, and a shrinkage function is assembled based on posterior probabilities. The shrinkage functions at consecutive scales are combined, and then applied to the wavelets coefficients. Given a resolution of analysis, the image denoising process is adaptive (i.e. do not require further parameter adjustments), and the selection of a gain factor provides the desired detail enhancement. The enhancement function was designed to avoid introducing artifacts in the enhancement process, which is essential in mammographic image analysis. Our preliminary results indicate that our method allows to detect microcalcifications and other suspicious structures in situations where their detection would be difficult otherwise. Compared to other approaches, our method requires less parameter adjustments by the user.*

**Keywords:** *mammography, image denoising, image enhancement, multiresolution analysis, wavelets.*

## 1. Introduction

Breast cancer currently accounts for more than 30% of cancer incidence, and a significant percentage of cancer mortality in both developing and developed countries. It has been shown that early detection and treatment of breast cancer are the most effective methods of reducing mortality.

Despite of advances in resolution and film contrast, screenfilm mammography remains a diagnostic imaging mo-dality where image interpretation is very difficult [7]. Breast radiographs are generally examined for the presence of malignant masses and indirect signs of malignancy such as the presence of microcalcifications and skin thickening. A significant effort has been directed to improve imaging performance, but it is unlikely that improvements will be achieved only by advances in screenfilm radiography.

In general, the visualization of mammograms displays a small percentage of the information available [7]. This deficiency of the mammographic technology is caused by the fact that, in general, there are small differences in x-ray attenuation between normal glandular and malignant tissues. Detection of small malignancies is specially difficult in younger women who tend to present denser breast tissue. On the other hand, calcifications have high attenuation properties (because these are denser tissues, similar to bones), but are small in size, and tend to present low local contrast. Therefore, the visibility of small tumors, and any associated microcalcifications, is a problem in the mammography technology based on analog film.

A very actual challenge is to improve the visual quality of mammograms by image processing in order to help in the early detection of breast cancer. Unfortunately, mammographic images are inherently noisy, and it is important to enhance image details without enhancing noise. Therefore, an important problem in mammographic image processing is to reduce noise in such images without blurring fine image details (i.e. image edges). Several approaches based on the wavelet transform have been proposed in the literature for this task.

Malfait and Roose [9] developed a filtering technique

Proceedings of the XVII Brazilian Symposium on Computer Graphics and Image Processing (SIBGRAPI'04)
1530-1834/04 $ 20.00 IEEE

that takes into account two image measurements. The first one measures the local regularity of the image using the Hölder exponent, and the second one takes into account geometric constraints. These two measures are combined in a Bayesian probabilistic framework, and implemented by as a Markov random field model. However, the stochastic sampling procedure, needed in the calculation of the probabilities, is computationally demanding.

In the approach of Chang *et al.* [1], coefficients associated with noise are modelled as Gaussian functions, while coefficients associated to edges are modelled as Generalized Gaussian functions. These probability functions are used to determine a soft threshold, which is applied to the wavelet coefficients. In a modification of this method [2], context modelling was introduced, and each coefficient is represented by a Generalized Gaussian random variable based on local spatial information. For each coefficient, a threshold is estimated.

Mihçak *et al.* [12] also proposed a spatially-adaptive statistical model for image denoising. Wavelet coefficients are modelled as Gaussian random variables with high local correlation, and a maximum *a posteriori* probability rule is applied to estimate the original coefficients from noisy observations. Strela *et al.* [15] described the joint densities of groups of wavelet coefficients as a Gaussian scale mixture (GSM), and developed a maximum likelihood solution for estimating relevant wavelet coefficients (i.e. related to edges) from noisy observations.

Portilla and Simoncelli [13] proposed a complex wavelet decomposition and processing for image denoising. The autocorrelations of theoretical noise-free coefficients and their magnitudes are estimated within each subband, and then projected onto spaces having the desired autocorrelations. The image is reconstructed with the modified coefficients, and this process is repeated iteratively, until a convergence is achieved. Figueiredo and Nowak [5] proposed a wavelet-based denoising technique without any free parameters, using empirical Bayes estimation based on a Jeffrey's noninformative prior.

The main problem of the approaches mentioned above (except for [5]) is that a noise estimate is needed, which may be difficult to obtain in practical situations, specially for images with inherent noise (e.g. x-ray images, aerial images, etc.). In fact, the reported probabilistic approaches [14, 1, 2, 12, 15, 13, 5] were not sufficiently tested for these types of images.

There are also known approaches designed specifically for mammographic image enhancement, and some of them are discussed next. Yoshida *et al.* [17] proposed to use the discrete wavelet transform (DWT), and multiply every scale by a weight factor, and then reconstruct an image using the inverse DWT. The weights are determined by supervised learning, given a set of training cases. However, the DWT is not translation invariant, meaning that a shift in the image origin leads to results inherently different to the transform applied to the original image. Laine *et al.* [8, 7] used a dyadic wavelet transform [10], and an adaptive enhancement operator on the wavelet coefficient scales. They obtained good contrast improvement for irregular structures such as microcalcifications and masses. The enhancement operation must be defined at each scale separately, and they do not exploit the correlation of wavelet coefficients across scales. Besides, it can be challenging to adjust parameters in order to obtain the desired results. Recently, Heinlein *et al.* [6] proposed a microcalcification enhancement method based on the continuous wavelet transform (CWT) and a local microcalcification model. Their method requires an empirical selection of appropriate thresholds for image denoising, as well as the specification of an appropriate size range for the structures to be enhanced. This method can not be applied for mammographic image enhancement in general, because the size and shape of the suspicious structures vary significantly in mammograms.

In this work, we propose a new adaptive method for mammographic image denoising and enhancement using the wavelet transform, which combines wavelet shrinkage and scale-space constraints. Our approach is flexible enough to allow the user to select the desired image enhancement and scale of analysis, but it does not require the user to adjust any parameters for image denoising. We adopt the approach proposed by Mallat and Zhong [11] to compute a redundant wavelet transform using only two detail images (horizontal and vertical), instead of the classical approach where three detail images are utilized (horizontal, vertical and diagonal details) [10]. This redundant wavelet transform is known to be virtually shift invariant. The distribution of detail coefficients is modelled by a composition of Gaussian and Generalized Gaussian probability density functions at each scale, a shrinkage function is assembled. Such shrinkage functions are combined in consecutive levels to preserve edges that are persistent over scales and remove residual noise. Finally, an adaptive piecewise linear enhancement function is applied to the denoised wavelet coefficients.

The next section gives a brief description of the wavelet framework, and the section that follows describes the new method. Section 4 presents some experimental results, and our conclusions are presented in the final section.

## 2. The Wavelet Transform

To compute the wavelet transform with two detail images, a smoothing function $\phi(x, y)$ and two wavelets $\psi^i(x, y)$ are needed. The dilation of these functions are de-

noted by

$$\phi_s(x,y) = \frac{1}{s^2}\phi(\frac{x}{s},\frac{y}{s}) \, , \psi^i_s(x,y) = \frac{1}{s^2}\psi^i(\frac{x}{s},\frac{y}{s}),\ i = 1,2, \tag{1}$$

and the dyadic wavelet transform $f(x,y)$, at a scale $s = 2^j$, has two detail components, given by

$$W^i_{2^j} f(x,y) = (f * \psi^i_{2^j})(x,y),\ i = 1,2, \tag{2}$$

and one low-pass component, given by

$$S_{2^j} f(x,y) = (f * \phi_{2^j})(x,y). \tag{3}$$

The coefficients $W^1_{2^j} f(x,y)$ and $W^2_{2^j} f(x,y)$ represent the details in the $x$ and $y$ directions, respectively. Thus, the image gradient at the resolution $2^j$ can be approximated by

$$\mathbf{W}_{2^j} f(x,y) = \begin{pmatrix} W^1_{2^j} f(x,y) \\ W^2_{2^j} f(x,y) \end{pmatrix}. \tag{4}$$

Since we are dealing with digital images $f[n,m]$, we use the discrete version of the wavelet transform [11], and the discrete wavelet coefficients are denoted in this paper by $W^i_{2^j} f[n,m]$, for $i = 1,2$.

## 3. Our Denoising-Enhancement Technique

Given a digital image $f[n,m]$, we apply the redundant wavelet transform using $J$ dyadic levels. As a result, we obtain $2J$ detail images $W^1_{2^j} f[n,m], W^2_{2^j} f[n,m]$, for $j = 1, ..., J$, and the smoothed image $S_{2^J} f[n,m]$.

Next, we describe our method to discriminate coefficients associated with edges from coefficients associated with noise based on *a posteriori* probabilities. We propagate this information in the scale-space (using consistency along scales), applying an adaptive piecewise linear enhancement function. Finally compute the inverse wavelet transform to obtain the processed image.

### 3.1. Wavelet Shrinkage

Wavelet shrinkage is a known approach for noise reduction, where wavelet coefficients are subject to a non-linearity that reduces (or suppresses) low-amplitude values, and retains high-amplitude values [14, 3].

For each level $2^j$, we want to find non-negative non-decreasing shrinkage functions $g^i_j(x)$, $0 \le g^i_j(x) \le 1$, such that the wavelet coefficients $W^1_{2^j} f$ and $W^2_{2^j} f$ are updated according to the following rule:

$$NW^i_{2^j} f[n,m] = W^i_{2^j} f[n,m] g^i_j[n,m], \quad i = 1,2, \tag{5}$$

where $g^i_j[n,m] = g^i_j(W^i_{2^j} f[n,m])$ are called *shrinkage factors*. Considering that the same shrinkage procedure (Equation (5)) will be applied at all scales and subbands of the wavelet decomposition, the indexes $j$ and $i$ will be used only when necessary.

To determine a shrinkage function $g(x)$, we analyze the distribution of coefficients $Wf[n,m]$. In this work, we model the mammographic image noise by an additive zero-mean Gaussian noise [6]. The detail coefficients $Wf[n,m]$ of an image constituted only by Gaussian noise may be considered Gaussian distributed [4], with standard deviation $\sigma_{\text{noise}}$. Under these circumstances, the function that models the coefficient distribution is given by

$$p(x|\text{noise}) = \frac{1}{\sigma_{\text{noise}}\sqrt{2\pi}} e^{-x^2/2\sigma^2_{\text{noise}}} \tag{6}$$

Therefore, $p(x|\text{noise})$ represents the distribution of coefficients assuming that only noise is present in the image.

On the other hand, the distribution of the wavelet coefficients for noise-free images is sharply peaked near the origin (due to homogeneous regions) and has a long tail (due to image edges). In fact, a more suitable function to model such coefficients is a Generalized Gaussian [14, 10]. Thus, we assume that the distribution of noise-free wavelet coefficients $Wf[n,m]$ is approximated by a Generalized Gaussian probability density function, given by:

$$\begin{aligned} &p(x|\text{edge}) = C(\beta,\sigma_{\text{edge}}) e^{-(\alpha(\beta,\sigma_{\text{edge}})|x|)^\beta}, \\ &\text{for } -\infty < x < \infty, \ \ \beta > 0, \ \ \sigma_{\text{edge}} > 0, \end{aligned} \tag{7}$$

where

$$\begin{aligned} \alpha(\beta,\sigma_{\text{edge}}) &= \sigma^{-1}_{\text{edge}} \left[\frac{\Gamma(\frac{3}{\beta})}{\Gamma(\frac{1}{\beta})}\right]^{1/2}, \\ C(\beta,\sigma_{\text{edge}}) &= \frac{\beta\alpha(\beta,\sigma_{\text{edge}})}{2\Gamma(\frac{1}{\beta})}, \end{aligned} \tag{8}$$

and $\Gamma(x)$ is the gamma function. Therefore, $p(x|\text{edge})$ represents the distribution of coefficients assuming that only edges and homogeneous regions are present in the image. The notation $p(x|\text{edge})$ was chosen because we are interested mostly in edges, as will be detailed below. The hypotheses of images containing *noise only* and *edge plus homogeneous regions only* are mutually exclusive. This is central to our approach, which models the generic coefficient distribution of images containing noisy edges and homogeneous regions affected by noise. We approximate the above mentioned generic coefficient distribution by a mixture of a Gaussian and a Generalized Gaussian distributions, as discussed next.

When we have an image contaminated by zero-mean additive Gaussian noise, the tail of the distribution will not be significantly affected by noise (because typically edge-related coefficients have magnitudes larger than noise-related coefficients). In this work, we assume that coefficients belonging to the tail of the distribution are likely to be edge-related, and coefficients close to the origin of the histogram are likely to be related to noise (and to nearly homogeneous regions). Hence, the origin of the histogram will

be Gaussian shaped, and the tail of the distribution will follow a Generalized Gaussian function, and the overall distribution of the coefficients $Wf[n,m]$ (including coefficients related to edges and noise) is given by

$$p(x) = wp(x|\text{noise}) + (1-w)p(x|\text{edge}), \qquad (9)$$

where $w$ is an unknown parameter of the overall coefficient distribution ($0 \leq w \leq 1$).

The parameters $\sigma_{\text{noise}}$, $\sigma_{\text{edge}}$, $\beta$ and $w$ are estimated by maximizing the likelihood function

$$\ln L = \sum_{(m,n) \text{ in image}} \ln\left(p(Wf[n,m])\right), \qquad (10)$$

where $p(Wf[n,m])$ is the function defined in Equation (9) evaluated at coefficients $Wf[n,m]$.

Typically, the variance of noise-related coefficients is smaller than the variance of edge-related coefficients. Also, noise variance decreases as $j$ increases (because of low-pass filtering). Therefore, the restrictions $\sigma_{\text{noise}} < \sigma_{\text{edge}}$ and $\sigma^j_{\text{noise}} \leq \sigma^{j-1}_{\text{noise}}$ are also imposed in the maximization procedure.

Once the parameters $\sigma_{\text{noise}}$, $\sigma_{\text{edge}}$, $\beta$ and $w$ are estimated, the conditional probability density functions $p(x|\text{noise})$ and $p(x|\text{edge})$ are given, respectively, by Eqs. (6) and (7). The shrinkage function $g(x)$ is given by the posterior probability function $p(\text{edge}|x)$, which is computed using Bayes theorem as follows:

$$g(x) = \frac{(1-w)p(x|\text{edge})}{(1-w)p(x|\text{edge}) + wp(x|\text{noise})} \qquad (11)$$

### 3.2. Consistency Along Scales

The analysis of the wavelet coefficients at each resolution does not provide sufficient discrimination between edge-related and noise-related coefficients, specially in the level $2^1$, where we find the highest noise contamination. Better discrimination can be achieved by analyzing the information available in different scales. Typically, consistency across scales is explored by computing the Lipschitz exponent of the wavelet coefficients [9], or the direct correlation of coefficients in consecutive scales [16]. In this work, we explore consistency across scales simply by combining shrinkage factors in adjacent scales, as described below.

For each scale $2^j$, the value $g_j[n,m]$ may be interpreted as a confidence measure that coefficient $W_{2^j}f[n,m]$ is in fact associated to an edge. To take into account multiple resolutions, we use the information provided by the shrinkage factor $g_j[n,m]$, and also by the factors $g_{j+1}[n,m]$, $g_{j+2}[n,m]$,...,$g_\kappa[n,m]$, where $\kappa - j + 1$ is the number of consecutive resolutions that will be taken into consideration for consistency along scales (the values assumed by $\kappa$ will be described below). We want to combine this information so that, if the value $g_j[n,m]$ is close to 1 for several consecutive levels $2^j$, it is more likely that $W_{2^j}f[n,m]$ is associated to an edge. On the other hand, if $g_j[n,m]$ decreases as $j$ increases, it is more likely that $W_{2^j}f[n,m]$ is actually associated with noise. We update the shrinkage factors according to the following rule:

$$g_j^{\text{scale}}[n,m] = \left(\frac{g_j[n,m]^\gamma + \cdots + g_\kappa[n,m]^\gamma}{\kappa - j + 1}\right)^{1/\gamma}, \qquad (12)$$

where $\gamma$ is a positive constant. When $\gamma = 1$, the average of the shrinkage factors is obtained. For $\gamma < 1$, smaller coefficients carry more weight, and tend to dominate the summation, producing smaller values. This means that when $\gamma$ is closer to zero, noise reduction is stronger, and when $\gamma$ is larger, edge preservation is stronger. It was verified experimentally that using $\gamma = 0.8$ for different test images (with distinct noise contamination levels), the expected difference in PSNR is smaller than $0.5$ dB with respect to the optimal PSNR (determined by exhaustive testing of different $\gamma$ values). Therefore, we used $\gamma = 0.8$ in our experiments with mammographic images.

Typically, when 2 or 3 consecutive resolutions are used, better results are obtained than when more consecutive resolutions are used. This is because the local extrema of $W^i_{2^j}f[n,m]$ tend to change their position as $2^j$ increases, as observed by Xu *et al.* [16].

This updating rule is applied from coarser to finer resolutions. The shrinkage factor $g_J^{\text{scale}}[n,m]$, corresponding to the coarsest resolution $2^J$, is equal to $g_J[n,m]$. However, for other resolutions $2^j$, $j = 1,...,J-1$, the shrinkage factors $g_j^{\text{scale}}[n,m]$ depend on scales $2^j, 2^{j+1}, ..., 2^\kappa$, where $\kappa = \min\{J, j+K\}$, and $K+1$ is the maximum number of consecutive scales that will be analyzed. The coefficients $W_{2^j}f[n,m]$ are then modified according to Equation (5), using the updated shrinkage factors $g_j^{\text{scale}}[n,m]$ instead of $g_j[n,m]$ [1].

### 3.3. Edge Enhancement

The denoising technique described above can be extended to local contrast enhancement near edges. Linear enhancement is straightforward, and can be obtained by allowing the shrinkage factors $g_j^{\text{scale}}[n,m]$ to be greater than 1, so that local contrast will be enhanced near the edges. Nevertheless, linear enhancement tends emphasize mostly strong edges, and mammograms enhanced by a linear operator containing an obvious macrocalcification (high intensity) will result in gross rescaling with the available dynamic range for image display [7].

1 The subband index $i$ was omitted here to simplify notation.

Laine *et al.* [7] proposed a nonlinear enhancement method with the following design guidelines in mind : (a) areas of low contrast are enhanced more than high contrast areas; (b) sharp edges are not blurred; (c) the enhancement function satisfies the constraints of monotonicity and antisymmetry. These guidelines provide that low contrast features will be more enhanced than the high contrast image features, and that artifacts will not be introduced by the enhancement method.

The proposed enhancement function $h_j^i$, which is used for updating the denoised wavelet coefficients $NW_{2^j}^i f[n,m]$, is given by the following rule:

$$h_j^i(x) = \begin{cases} x - (G-1)T_{2^j}^i, & \text{if } x < -T_{2^j}^i \\ G \cdot x, & \text{if } |x| < T_{2^j}^i \\ x + (G-1)T_{2^j}^i, & \text{if } x > T_{2^j}^i \end{cases}, \qquad (13)$$

where $T_{2^j}^i$ is the *median* of coefficient magnitudes $|NW_{2^j}^i|$ at the corresponding scale $j$ and subband $i$, and $G \geq 1$. Laine *et al.* [7] use a similar nonlinear enhancement method, but in their approach $T_{2^j}^i$ must be user specified, which can be quite troublesome in practical situations. Our approach is adaptive, and only requires the user to select the desired enhancement level $G$.

Finally, the enhanced wavelet coefficients are computed by:

$$NW_{2^j{}_{\text{enh}}}^i f[n,m] = h_j^i(NW_{2^j}^i f[n,m]), \qquad (14)$$

and the inverse wavelet transform is applied to obtain the denoised-enhanced image.

## 4. Experimental Results

We have implemented our method in MATLAB, and tested our approach on the mammograms of the MIAS database (*http://peipa.essex.ac.uk/info/mias.html*). These images are available from this database in reduced resolution, as compared to conventional digital mammograms. Therefore, we used only 2 dyadic scales in our analysis. Also, we normalized the image grayscale range (i.e. $[0, 255]$), and used $G = 7$ for all images tested (different degrees of enhancement could be used, but this would make difficult to compare the results).

In order to further enhance the image details, and deenhance homogeneous regions, in our experiments we also computed an *unsharp masking* version of our method:

$$f_{\text{unsharp}}[n,m] = 2 \cdot f_{\text{enh}}[n,m] - f[n,m] \qquad (15)$$

where, $f_{\text{enh}}[n,m]$ and $f[n,m]$ are the image enhanced by our approach and the original image, respectively. Next, some of our preliminary experimental results are discussed.

As mentioned in Section 1, the early detection and treatment of breast cancer are the most effective methods of reducing mortality. Therefore, any early signs of abnormality should be detected in mammograms. Figure 1(a) shows the MIAS database mammogram *211* containing a low contrast cluster of small microcalcifications surrounded by dense tissues (bright image region), at the bottom right. Altohugh the shape and geometry of these microcalcifications are suspicious, they are not clearly visible in a first evaluation. However, they should be inspected by the diagnosing specialist. Our approach denoises and improves local contrast, showing more clearly this cluster of microcalcifications as displayed in Figure 1(b); also, Figure 1(c) shows the unsharp masking results, where the details of this cluster of small microcalcifications are even more visible (bottom right). Similar comments apply to the local contrast enhancement of microcalcifications occurring in mammograms *265* and *148*, whose results are displayed in Figures 2 and 3, respectively. Please, observe the *ductiform* shape of the microcalcifications clusters in Figure 3(b) and 3(c), which provide relevant diagnostic information.

Figure 4(a) shows the MIAS database mammogram *145*, which contains a low contrast suspicious mass with spiculated borders, surrounded by dense tissues near the image top. The low contrast borders of this suspicious mass must be inspected by a diagnosing specialist, and can be seen with higher local contrast in Figure 4(b), and are shown even more clearly in Figure 4(c).

Our preliminary experimental results indicate that our method can help denoising and improving local contrast in digital mammograms. These image improvements are important for early detection and risk evaluation posed by microcalcifications and suspicious masses found in such images.

## 5. Conclusions

To improve visual quality of mammograms by image processing in order to help early detection of breast cancer is a current research challenge.

This paper describes a new method for mammographic image noise suppression and enhancement based on the wavelet transform. The image denoising process is adaptive, and the selection of a gain factor provides the desired detail enhancement. Our method was designed to avoid introducing artifacts in the enhancement process, which is very important to analyze digital mammograms reliably. The preliminary results indicate that our method improves the detection of microcalcifications and other suspicious structures, even in situations where their detection is difficult (e.g. in low contrast image regions, near dense tissues). Compared to other approaches, our method requires less user adjustment parameters.

In the continuation of this work, we intend to evaluate our approach in clinical trials designed by mammography specialists. Despite of Gaussian noise models being widely

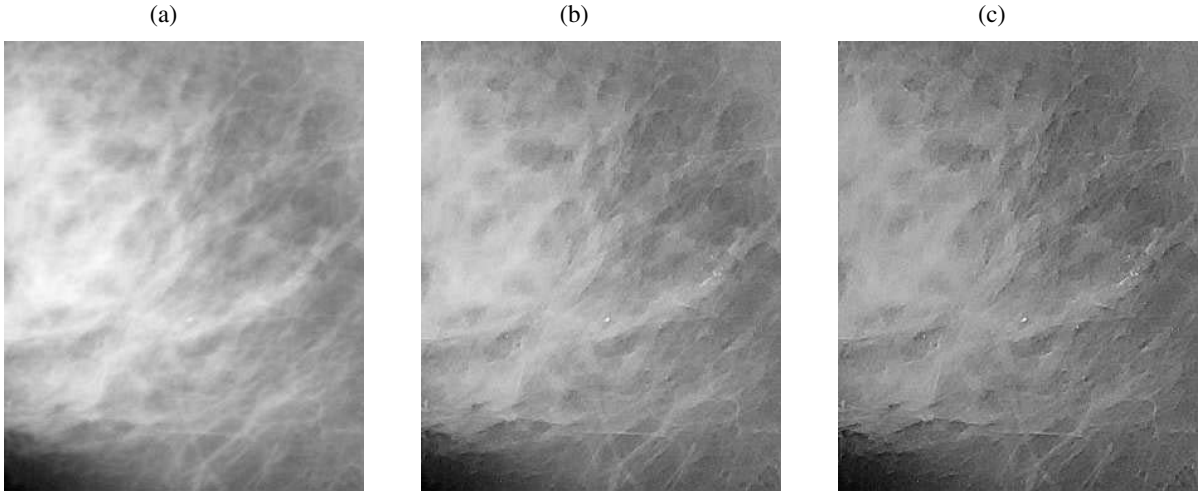


**Figure 1. Comparative results for the MIAS database mammogram *211*, containing a small cluster of microcalcifications which is not clearly visible in denser areas, at the bottom right. (a) original image; (b) image enhanced using our approach (the small cluster of microcalcifications is more visible in the bottom right); and (c) unsharp masking of the original image (the small cluster of microcalcifications is visible in the bottom right).**

accepted, we intend to extend our denoising approach to include also non-Gaussian noise.

## References


[1] S. G. Chang and M. Vetterli. Spatial adaptive wavelet thresholding for image denoising. In *Proc. 1997 International Conference on Image Processing (ICIP97)*, pages 374–377, 1997.

[2] S. G. Chang, B. Yu, and M. Vetterli. Spatially adaptive wavelet thresholding with context modeling for image denoising. *IEEE Transactions on Image Processing*, 9(9):1522–1531, September 2000.

[3] D. L. Donoho. Nonlinear wavelet methods for recovery of signals, densities and spectra from indirect and noisy data. In I. Daubechies, editor, *Proc. Symposium on Applied Mathematics*, volume 47, pages 173–205, Providence, RI, 1993.

[4] D. L. Donoho. Wavelet shrinkage and w.v.d.: A 10-minute tour. *Progress in Wavelet Analysis and Applications*, 1993.

[5] M. A. T. Figueiredo and R. D. Nowak. Wavelet-based image estimation: An empirical bayes approach using jeffrey's noninformative prior. 10(9):1322–1331, September 2001.

[6] P. Heinlein, J. Drexl, and W. Schneider. Integrated wavelets for enhancement of microcalfications in digital mammography. *IEEE Transactions on Medical Imaging*, 22(3):402–413, March 2003.

[7] A. Laine, J. Fan, and W. Yang. Wavelets for contrast enhancement of digital mammography. *IEEE Engineering in Medicine and Biology*, 14(5):536–550, September / October 1995.

[8] A. Laine, S. Schuler, J. Fan, and W. Huda. Mammographic feature enhancement by multiscale analysis. *IEEE Transactions on Medical Imaging*, 13(4):725–740, December 1994.

[9] M. Malfait and D. Roose. Wavelet based image denoising using a Markov Random Field a priori model. *IEEE Transactions on Image Processing*, 6(4):549–565, 1997.

[10] S. G. Mallat. A theory for multiresolution signal decomposition: The wavelet representation. *IEEE Transactions on Pattern Analysis and Machine Intelligence*, 11(7):674–693, 1989.

[11] S. G. Mallat and S. Zhong. Characterization of signals from multiscale edges. *IEEE Transactions on Pattern Analysis and Machine Intelligence*, 14(7):710–732, 1992.

[12] M. K. Mihçak, I. Kozintsev, K. Ramchandram, and P. Moulin. Low-complexity image denoising based on statistical modeling of wavelet coefficients. *IEEE Signal Processing Letters*, 6(12):300–303, December 1999.

[13] J. Portilla and E. P. Simoncelli. Image denoising via adjustment of wavelet coefficient magnitude correlation. In *Proc. 7th International Conference on Image Processing*, volume 3, pages 277–280, Vancouver, BC, Canada, September 2000.

[14] E. P. Simoncelli and E. Adelson. Noise removal via bayesian wavelet coring. In *Proc. IEEE International Conference on Image Processing*, pages 279–382, Lausanne, Switzerland, September 1996.

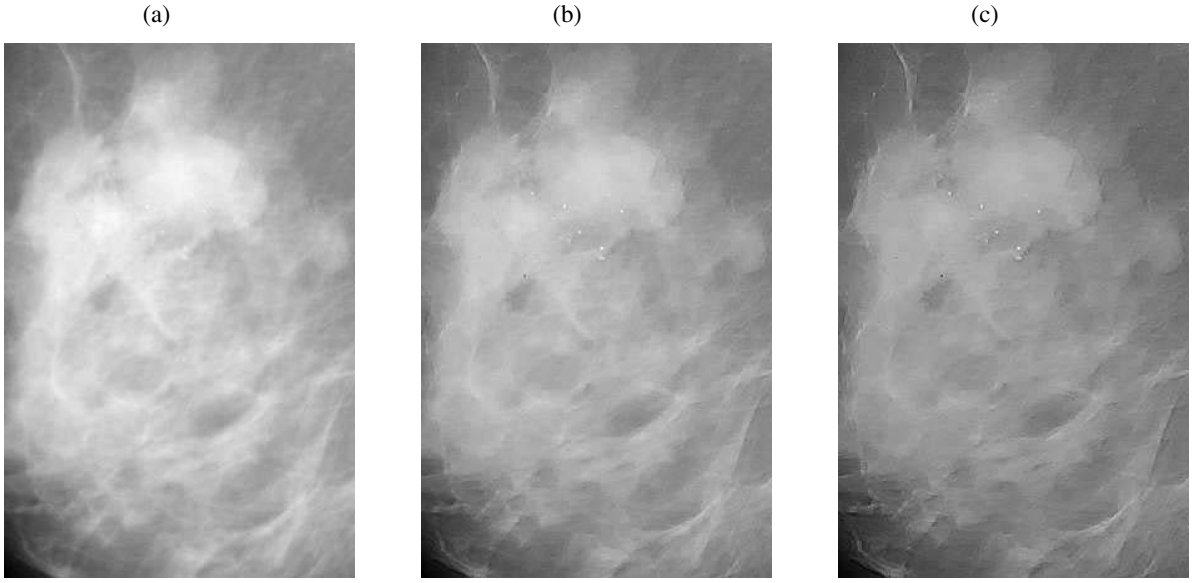


**Figure 2. Comparative results for the MIAS database mammogram *265*, containing a cluster of microcalcifications whose geometry is not clearly visible near the image center. (a) original image; (b) image enhanced using our approach (the microcalcifications cluster is more visible near the image center); and (c) unsharp masking of the original image (the microcalcifications cluster is visible near the image center).**

[15] V. Strela, J. Portilla, and E. P. Simoncelli. Image denoising via a local gaussian scale mixture model in the wavelet domain. In *Proc. SPIE 45th Annual Meeting*, San Diego, CA, August 2000.

[16] Y. Xu, J. B. Weaver, D. M. Healy, and J. Lu. Wavelet transform domain filters: A spatially selective noise filtration technique. *IEEE Transactions on Image Processing*, 3(6):747–758, 1994.

[17] H. Yoshida, W. Zhang, W. Cai, K. Doi, R. M. Nishikawa, and M. L. Giger. Optimizing wavelet transform based on supervised learning for detection of microcalcifications in digital mammograms. In *Proc. IEEE International Conference on Image Processing*, pages 152–155, Lausanne, Switzerland, September 1996.

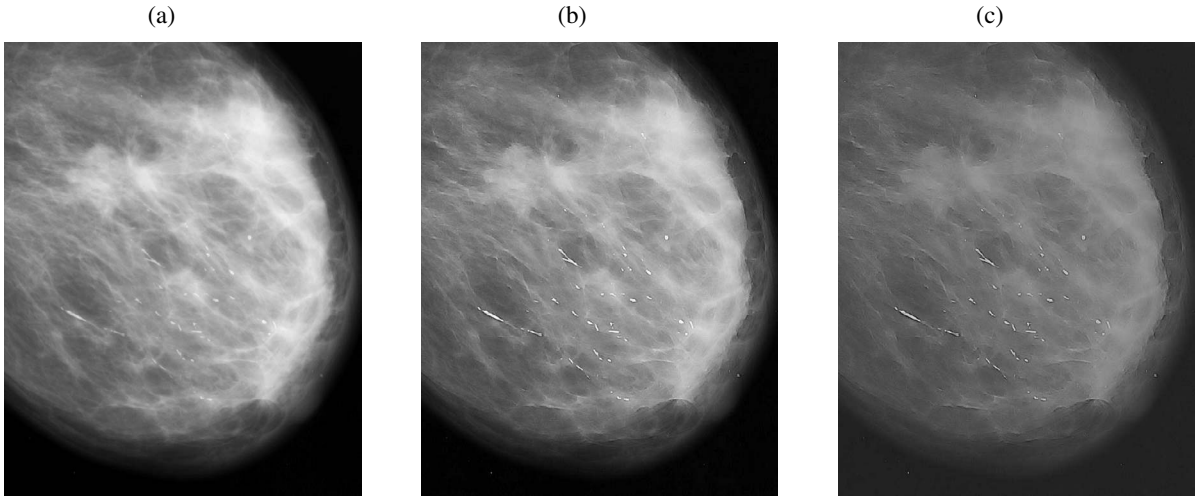


**Figure 3. Comparative results for the MIAS database mammogram *148*, containing several suspicious microcalcifications which are not clearly visible, mostly in the denser areas. (a) original image; (b) image enhanced using our approach (showing details of the microcalcifications, including those located in denser areas); and (c) unsharp masking of the original image (the details of the microcalcifications are visible, including those located in denser areas).**

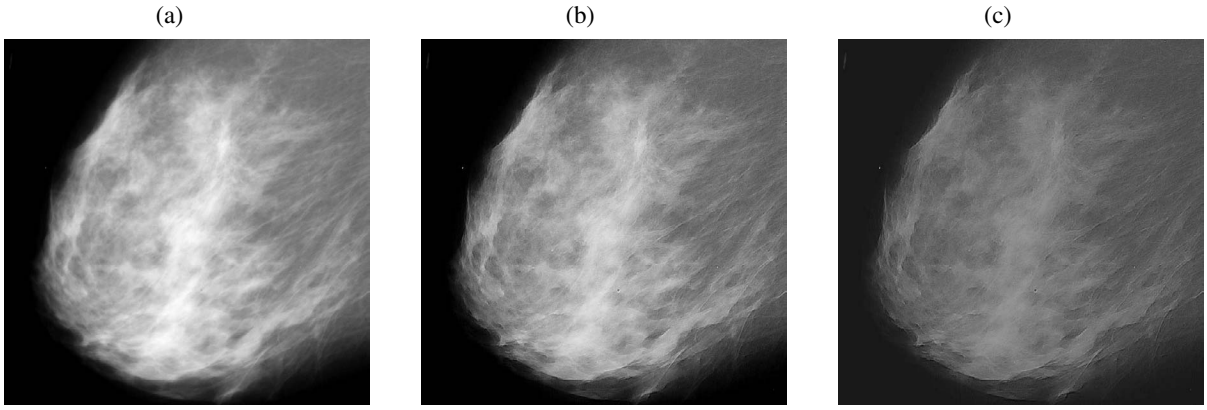


**Figure 4. Comparative results for the MIAS database mammogram *145*, containing a suspicious mass with spiculated borders which are not clearly visible, located near the image top. (a) original image; (b) image enhanced using our approach (the spiculated borders of the suspicious mass are more visible, near the image top); and (c) unsharp masking of the original image (the spiculated borders of the suspicious mass are visible, near the image top).**